Article

Quantum Tunneling and Quantum Phase Interference in a [MnMn] Single-Molecule Magnet

Lollita Lecren, Wolfgang Wernsdorfer, Yang-Guang Li, Olivier Roubeau, Hitoshi Miyasaka, and Rodolphe Clrac

J. Am. Chem. Soc., **2005**, 127 (32), 11311-11317• DOI: 10.1021/ja050994z • Publication Date (Web): 21 July 2005

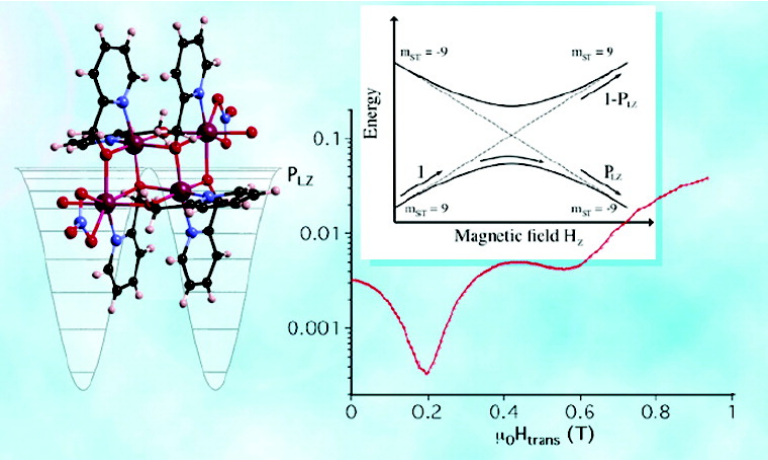

More About This Article

Additional resources and features associated with this article are available within the HTML version:

- Supporting Information
- Links to the 10 articles that cite this article, as of the time of this article download
- Access to high resolution figures
- Links to articles and content related to this article
- Copyright permission to reproduce figures and/or text from this article

View the Full Text HTML

J|A|C|S
ARTICLES
Published on Web 07/21/2005

Quantum Tunneling and Quantum Phase Interference in a $[Mn^{II}_2Mn^{III}_2]$ Single-Molecule Magnet

Lollita Lecren,[†] Wolfgang Wernsdorfer,*[,‡] Yang-Guang Li,[†,||] Olivier Roubeau,[†] Hitoshi Miyasaka,*[,§] and Rodolphe Clérac*[,†]

Contribution from the Centre de Recherche Paul Pascal, CNRS UPR-8641, 115 av. du Dr. Albert Schweitzer, 33600 Pessac, France, Laboratoire Louis Néel, CNRS, BP 166, 25 av. des Martyrs, 38042 Grenoble, France, Department of Chemistry, Graduate School of Science, Tokyo Metropolitan University, 1-1 Minami-ohsawa, Hachioji, Tokyo 192-0397, Japan, and PRESTO and CREST, Japan Science and Technology Agency, 4-1-8 Honcho, Kawaguchi, Saitama 332-0012, Japan

Received February 16, 2005; E-mail: clerac@crpp-bordeaux.cnrs.fr; miyasaka@comp.metro-u.ac.jp; wernsdor@grenoble.cnrs.fr

Abstract: $[Mn_4(hmp)_6(H_2O)_2(NO_3)_2](NO_3)_2\cdot 2.5H_2O$ (**1**) has been synthesized from the reaction of 2-hydroxymethylpyridine (Hhmp) with $Mn(NO_3)_2\cdot 4H_2O$ in the presence of tetraethylammonium hydroxide. **1** crystallizes in the triclinic $P\bar{1}$ space group with two crystallographically independent centrosymmetrical $[Mn_4(hmp)_6(H_2O)_2(NO_3)_2]^{2+}$ complexes in the packing structure. Four Mn ions are arranged in a double-cuboidal fashion where outer Mn^{2+} are heptacoordinated and inner Mn^{3+} are hexacoordinated. dc magnetic measurements show that both $Mn^{2+}\cdots Mn^{3+}$ and $Mn^{3+}\cdots Mn^{3+}$ interactions are ferromagnetic with $J_{wb}/k_B = +0.80(5)$ K, and $J_{bb}/k_B = +7.1(1)$ K, respectively, leading to an $S_T = 9$ ground state. Combined ac and dc measurements reveal the single-molecule magnet (SMM) behavior of **1** with both thermally activated and ground-state tunneling regimes, including quantum phase interference. In the thermally activated regime, the characteristic relaxation time (τ) of the system follows an Arrhenius law with $\tau_0 = 6.7 \times 10^{-9}$ s and $\Delta_{eff}/k_B = 20.9$ K. Below 0.34 K, τ saturates indicating that the quantum tunneling of the magnetization becomes the dominant relaxation process as expected for SMMs. Down to 0.04 K, field dependence of the magnetization measured using the μ-SQUID technique shows the presence of very weak inter-SMM interactions ($zJ'/k_B \approx -1.5 \times 10^{-3}$ K) and allows an estimation of D/k_B at -0.35 K. Quantum phase interference has been used to confirm the D value and to estimate the transverse anisotropic parameter to $E/k_B = +0.083$ K and the ground-state tunnel splitting $\Delta_{LZ} = 3 \times 10^{-7}$ K at $H_{trans} = 0$ Oe. These results rationalize the observed tunneling time (τ_{QTM}) and the effective energy barrier (Δ_{eff}).

Introduction

Since the discovery of the first single-molecule magnet (SMM) in the early 1990s,[1] a large community of chemists and physicists have worked together to discover new SMM complexes based on Mn,[2] Fe,[3] Ni,[4] V,[5] Co,[6] or mixed metals[7] polynuclear complexes and to probe their unique physical properties.[8] This field of research has become very active due to the fundamental questions raised by these systems at the frontier between classical and quantum physics and also as a result of the possible applications in terms of information storage and quantum computation.[8,9] At low temperatures, these nano-sized magnets exhibit slow relaxation of their magnetization, which is induced by a combined effect of their uniaxial anisotropy ($D < 0$) and high-spin ground state (S_T). These two characteristics create an energy barrier (Δ), equal to $|D|S_T^2$ for integer spins and $|D|(S_T^2 - {}^1/_4)$ for half-integer spins, between the two thermodynamically equivalent spin configurations $m_S = \pm S_T$. Hence, below T_B, the so-called blocking temperature, the thermal energy is not able anymore to overcome the barrier Δ, and the spin is trapped in one of the two equivalent configurations. This molecular property can be detected at the bulk level when a magnetic field is applied, saturating the magnetization below T_B. When this field is switched off, the magnetization slowly relaxes with a characteristic relaxation time (τ), which can be measured as a function of temperature using the time dependence of the magnetization and the frequency dependence of the ac susceptibility. This relaxation time follows a thermally activated behavior (Arrhénius law):

$$\tau(T) = \tau_0 \exp\left(\frac{\Delta}{k_B T}\right) \quad (1)$$

where τ_0 is a pre-exponential factor that is characteristic of a given molecular system and k_B is the Boltzmann constant. This slow relaxation of the magnetization leads to hysteresis effects

[†] Centre de Recherche Paul Pascal.
[‡] Laboratoire Louis Néel.
[§] Tokyo Metropolitan University, CREST, and PRESTO.
[||] Present address: Faculty of Chemistry, Northeast Normal University, Changchun, 130024, China.

(1) (a) Boyd, P. D. W.; Li, Q.; Vincent, J. B.; Folting, K.; Chang, H.-R.; Streib, W. E.; Huffman, J. C.; Christou, G.; Hendrickson, D. N. *J. Am. Chem. Soc.* **1988**, *110*, 8537. (b) Caneschi, A.; Gatteschi, D.; Sessoli, R. *J. Am. Chem. Soc.* **1991**, *113*, 5873. (c) Sessoli, R.; Tsai, H.-L.; Schake, A. R.; Wang, S.; Vincent, J. B.; Folting, K.; Gatteschi, D.; Christou, G.; Hendrickson, D. N. *J. Am. Chem. Soc.* **1993**, *115*, 1804.

with an applied field, signature of a magnetlike behavior. In contrast to a 3D ordered magnet where the presence of a coercive field is induced by a collective phenomenon, this effect originates solely from individual molecules in SMM materials.

At low temperature, the simplest model to describe an SMM, when only its ground-state S_T is thermally populated, has the following Hamiltonian:

$$H = DS_{Tz}^2 + E(S_{Tx}^2 - S_{Ty}^2) + g\mu_B\mu_0\vec{S}_T\cdot\vec{H} \qquad (2)$$

where S_T is the ground-state spin operator; S_{Tx}, S_{Ty}, and S_{Tz} are the three components of S_T; E is the transverse anisotropy, and hence the x, y, and z axes are, respectively, the hard, intermediate, and easy axes of the magnetization; μ_B is the Bohr magneton; and g is the Landé factor. At low enough temperature, a temperature-independent quantum regime can be experimentally observed as it becomes faster than the thermally activated relaxation. In zero field, states with $\pm m_S$ quantum numbers having the same energy, quantum tunneling of the magnetization between these pairs of levels is possible. In other words, this quantum mechanism allows individual nanomagnets to reverse their spin and therefore the magnetization of the material to relax to equilibrium. When a longitudinal field, H_z, is applied, $m_S < 0$ and $m_S > 0$ levels decrease and increase, respectively, in energy. Thus, quantum tunneling is not possible anymore between $\pm m_S$ states except for particular magnetic fields:

$$\mu_0 H_z^{(n)} \approx nD/(g\mu_B) \text{ with } n \text{ as an integer} \qquad (3)$$

at which "resonant quantum tunneling" is observed when two m_S states of opposite signs are raised at the same energy (Scheme 1).[8b]

When sweeping the longitudinal field, the tunnel rate of relaxation becomes periodically faster than the thermal pathway creating steps on the M versus H_z curve at each particular value of $H_z^{(n)}$. With this technique, the axial anisotropy, D, can be easily estimated. This simple picture explaining the quantum tunneling of the magnetization in SMMs does not reflect the primordial role played by the transverse anisotropy, E, which indeed governs this relaxation mode. The transverse anisotropy term, $E(S_{Tx}^2 - S_{Ty}^2)$, mixes the m_S states and creates a gap (Δ_{LZ}) at the crossings of the m_S levels (Scheme 1b). Indeed, Δ_{LZ}, also called the tunnel splitting, makes possible the quantum pathway of relaxation. This splitting induces a tunnel probability (P_{LZ}), which quantifies the proportion of spins that can be reversed. Moreover, this probability, which is measured by sweeping the longitudinal field, can be modulated by applying simultaneously a transverse field (H_{trans}) in the hard-intermediate plane (xy). The experimental tunnel splitting can be determined from the Laudau−Zener equation:[9a]

$$\Delta_{LZ} = \sqrt{-\frac{2\hbar\mu_B\mu_0}{\pi}|m_S - m_{S'}|\ln(1 - P_{LZ})\frac{dH_z}{dt}} \qquad (4)$$

where m_S and $m_{S'}$ are the quantum numbers of the two involved levels, dH_z/dt is the longitudinal field sweep rate, and $\hbar$ is Planck's constant. Measuring the tunnel probability (P_{LZ}) allows therefore to estimate very small tunnel splittings ($>10^{-9}$ K), not accessible with spectroscopic techniques. When applying a transverse field along the hard direction, oscillations of P_{LZ} are observed that are due to constructive or destructive quantum spin phase interference of two tunnel paths (Scheme 1c).[9a,10] Considering the previous Hamiltonian (eq 2), the oscillation period is given by:[10]

$$\Delta H_{LZ} = 2k_B\sqrt{2E(E + |D|)}/(g\mu_B) \qquad (5)$$

The transverse anisotropy E can thus be obtained with accuracy by measuring the quantum phase interference. To date, only two SMMs, $[Fe_8O_2(OH)_{12}(tacn)_6]^{8+}$ (where tacn is the 1,4,7-triazacyclononane) and $[Mn_{12}O_{12}(O_2CR)_{16}(H_2O)_4]^{n-}$ (with $n = 0$, 1, or 2, and where RCO_2^- is a carboxylate derivatives),

(2) (a) Aubin, S. M. J.; Wemple, M. W.; Adams, D. M.; Tsai, H.-L.; Christou, G.; Hendrickson, D. N. *J. Am. Chem. Soc.* **1996**, *118*, 7746. (b) Yoo, J.; Brechin, E. K.; Yamaguchi, A.; Nakano, M.; Huffman, J. C.; Maniero, A. L.; Brunel, L.-C.; Awaga, K.; Ishimoto, H.; Christou, G.; Hendrickson, D. N. *Inorg. Chem.* **2000**, *39*, 3615. (c) Boskovic, C.; Brechin, E. K.; Streib, W. E.; Folting, K.; Hendrickson, D. N.; Christou, G. *J. Am. Chem. Soc.* **2002**, *124*, 3725. (d) Brechin, E. K.; Boskovic, C.; Wernsdorfer, W.; Yoo, J.; Yamaguchi, A.; Sañudo, E. C.; Concolino, T.; Rheingold, A. L.; Ishimoto, H.; Hendrickson, D. N.; Christou, G. *J. Am. Chem. Soc.* **2002**, *124*, 9710. (e) Brechin, E. K.; Soler, M.; Davidson, J.; Hendrickson, D. N.; Parsons, S.; Christou, G. *Chem. Commun.* **2002**, 2252. (f) Boskovic, C.; Bircher, R.; Tregenna-Piggott, P. L. W.; Güdel, H. U.; Paulsen, C.; Wernsdorfer, W.; Barra, A.-L.; Khatsko, E.; Neels, A.; Stoeckli-Evans, H. *J. Am. Chem. Soc.* **2003**, *125*, 14046. (g) Miyasaka, H.; Clérac, R.; Wernsdorfer, W.; Lecren, L.; Bonhomme, C.; Sugiura, K.; Yamashita, M. *Angew. Chem., Int. Ed.* **2004**, *43*, 2801. (h) Tasiopoulos, A. J.; Vinslava, A.; Wernsdorfer, W.; Abboud, K. A.; Christou, G. *Angew. Chem., Int. Ed.* **2004**, *43*, 2117. (i) Murugesu, M.; Habrych, M.; Wernsdorfer, W.; Abboud, K. A.; Christou, G. *J. Am. Chem. Soc.* **2004**, *126*, 4766. (j) Soler, M.; Wernsdorfer, W.; Folting, K.; Pink, M.; Christou, G. *J. Am. Chem. Soc.* **2004**, *126*, 2156. (k) Murugesu, M.; Raftery, J.; Wernsdorfer, W.; Christou, G.; Brechin, E. K. *Inorg. Chem.* **2004**, *43*, 4203. (l) Sañudo, E. C.; Wernsdorfer, W.; Abboud, K. A.; Christou, G. *Inorg. Chem.* **2004**, *43*, 4137. (m) Wittick, L. M.; Murray, K. S.; Moubaraki, B.; Batten, S. R.; Spiccia, L.; Berry, K. *J. Chem. Soc., Dalton Trans.* **2004**, 1003.

(3) (a) Delfs, C.; Gatteschi, D.; Pardi, L.; Sessoli, R.; Wieghardt, K.; Hanke D. *Inorg. Chem.* **1993**, *32*, 3099. (b) Barra, A. L.; Caneschi, A.; Cornia, A.; Fabrizi de Biani, F.; Gatteschi, D.; Sangregorio, C. Sessoli, R.; Sorace, L. *J. Am. Chem. Soc.* **1999**, *121*, 5302. (c) Gatteschi, D.; Sessoli, R.; Cornia, A. *Chem. Commun.* **2000**, 725. (d) Oshio, H.; Hoshino, N.; Ito, T. *J. Am. Chem. Soc.* **2000**, *122*, 12602. (e) Benelli, C.; Cano, J.; Journaux, Y.; Sessoli, R.; Solan, G. A.; Winpenny, R. E. P. *Inorg. Chem.* **2001**, *40*, 188. (f) Goodwin, J. C.; Sessoli, R.; Gatteschi, D.; Wernsdorfer, W.; Powell, A. K.; Heath, S. L. *J. Chem. Soc., Dalton Trans.* **2000**, 1835. (g) Oshio, H.; Hoshino, N.; Ito, T.; Nakano, M. *J. Am. Chem. Soc.* **2004**, *126*, 8805.

(4) (a) Cadiou, C.; Murrie, M.; Paulsen, C.; Villar, V.; Wernsdorfer, W.; Winpenny, R. E. P. *Chem. Commun.* **2001**, 2666. (b) Andres, H.; Basler, R.; Blake, A. J.; Cadiou, C.; Chaboussant, G.; Grant, C. M.; Güdel, H.-U.; Murrie, M.; Parsons, S.; Paulsen, C.; Semadini, F.; Villar, V.; Wernsdorfer, W.; Winpenny, R. E. P. *Chem.−Eur. J.* **2002**, *8*, 4867. (c) Yang, E.-C.; Wernsdorfer, W.; Hill, S.; Edwards, R. S.; Nakano, M.; Maccagnano, S.; Zakharov, L. N.; Rheingold, A. L.; Christou, G.; Hendrickson, D. N. *Polyhedron* **2003**, *22*, 1727. (d) Moragues-Cánovas, M.; Helliwell, M.; Ricard, L.; Rivière, E.; Wernsdorfer, W.; Brechin, E.; Mallah, T. *Eur. J. Inorg. Chem.* **2004**, 2219.

(5) Castro, S. L.; Sun, Z.; Grant, C. M.; Bollinger, J. C.; Hendrickson, D. N.; Christou, G. *J. Am. Chem. Soc.* **1998**, *120*, 2365.

(6) Yang, E.; Hendrickson, D. N.; Wernsdorfer, W.; Nakano, M.; Zakharov, L. N.; Sommer, R. D.; Rheingold, A. L.; Ledezma-Gairaud, M.; Christou, G. *J. Appl. Phys.* **2002**, *91*, 7382.

(7) (a) Schake, A. R.; Tsai, H.-L.; Webb, R. J.; Folting, K.; Christou, G.; Hendrickson D. N. *Inorg. Chem.* **1994**, *33*, 6020. (b) Sokol, J. J.; Hee, A. G.; Long, J. R. *J. Am. Chem. Soc.* **2002**, *124*, 7656. (c) Karasawa, S.; Zhou, G.; Morikawa, H.; Koga, N. *J. Am. Chem. Soc.* **2003**, *125*, 13676. (d) Choi, H. J.; Sokol, J. J.; Long, J. R. *Inorg. Chem.* **2004**, *43*, 1606. (e) Osa, S.; Kido, T.; Matsumoto, N.; Re, N.; Pochaba, A.; Mrozinski, J. *J. Am. Chem. Soc.* **2004**, *126*, 420. (f) Zaleski, C. M.; Depperman, E. C.; Kampf, J. W.; Kirk, M. L.; Pecoraro, V. L. *Angew. Chem., Int. Ed.* **2004**, *43*, 3912. (g) Miyasaka, H.; Nezu, T.; Sugimoto, K.; Sugiura, K.; Yamashita, M.; Clérac, R. *Chem.−Eur. J.* **2005**, *11*, 1592. (h) Oshio, H.; Nihei, M.; Koizumi, S.; Shiga, T.; Nojiri, H.; Nakano, M.; Shirakawa, N.; Akatsu, M. *J. Am. Chem. Soc.* **2005**, *127*, 4568. (i) Oshio, H.; Nihei, M.; Yoshida, A.; Nojiri, H.; Nakano, M.; Yamaguchi, A.; Karaki, Y.; Ishimoto, H. *Chem.−Eur. J.* **2005**, *11*, 843. (j) Ferbinteanu, M.; Miyasaka, H.; Wernsdorfer, W.; Nakata, K.; Sugiura, K.; Yamashita, M.; Coulon, C.; Clérac, R. *J. Am. Chem. Soc.* **2005**, *127*, 3090.

(8) (a) Christou, G.; Gatteschi, D.; Hendrickson, D. N.; Sessoli, R. *MRS Bull.* **2000**, *25*, 66. (b) Gatteschi, D.; Sessoli, R. *Angew. Chem., Int. Ed.* **2003**, *42*, 268. (c) Ritter, S. K. *Chem. Eng. News* **2004**, *82*, 29.

(9) (a) Wernsdorfer, W.; Sessoli, R. *Science* **1999**, *284*, 133. (b) Leuenberger, M. N.; Loss, D. *Nature* **2001**, *410*, 789.

(10) Garg, A. *Europhys. Lett.* **1993**, *22*, 205.

Scheme 1. Quantum Tunneling of the Magnetization[a]

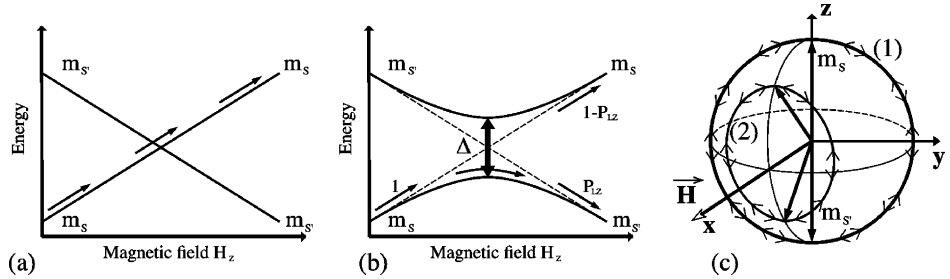

[a] Effect of the transverse anisotropy on the level crossing with $E = 0$ (a) and $E \neq 0$ (b); (c) semiclassical view emphasizing the two symmetrical tunnel paths of the quantum tunneling (clockwise and counterclockwise) (1) without applied field (the paths are in the *zy* plane) and (2) with a field applied along the *x* axis, the hard direction (the paths are in a plane parallel to the *zy* plane).

are known to exhibit quantum phase interference and have been studied in detail.[9a,11] Herein we report on a new Mn^{III}/Mn^{II} tetranuclear complex, $[Mn_4(hmp)_6(H_2O)_2(NO_3)_2](NO_3)_2 \cdot 2.5H_2O$ (**1**) (where hmp is the 2-hydroxymethylpyridine anion), exhibiting SMM behavior with thermally activated and ground-state tunneling regimes including quantum phase interference.

Experimental Section

Synthesis of 1. All chemicals and solvents used in the syntheses were reagent grade. $Mn(NO_3)_2 \cdot 4H_2O$ (0.346 g, 1.38 mmol), 2-hydroxymethylpyridine (Hhmp) (0.378 g, 3.45 mmol), and 20 wt % water solution of $[(CH_3CH_2)_4N]OH$ (0.530 g, 0.72 mmol) were successively dissolved in 20 mL of CH_3CN with stirring. After 1 h, the pink solution was filtrated, layered with diethyl ether, and kept in a sealed flask. Red-brown needlelike crystals were isolated after 7 days, collected by filtration, washed with a toluene/CH_3CN (4/1) mixture, and dried in air (Yield: 19%). Anal. Calcd. for $C_{36}H_{45}Mn_4N_{10}O_{22.5}$: C, 36.10; H, 3.79; N, 11.70. Found: C, 36.55; H, 4.50; N, 11.64. Selected IR data (KBr, cm^{-1}): 3414 (s), 2846 (m), 1600 (s), 1567 (s), 1479 (m), 1435 (m), 1387 (s), 1286 (m), 1218 (w), 1150 (m), 1062 (m), 1039 (s), 822 (s), 766 (s), 719 (m), 675 (m), 643 (m), 568 (s), 533 (m), 482 (w).

Physical Measurements. Elemental analyses (C, H, and N) were measured by Service Central d'Analyse of CNRS. IR spectra were recorded in the range 400−4000 cm^{-1} on a Nicolet 750 Magna-IR spectrometer using a KBr pellet. Magnetic susceptibility measurements were obtained with the use of a Quantum Design SQUID magnetometer (MPMS-XL). dc measurements were conducted from 1.8 to 300 K and from −70 to 70 kOe. ac measurements were performed at frequencies ranging from 0.1 to 1500 Hz with an ac field amplitude of 3 Oe and no dc field applied. The measurements were performed on finely ground polycrystalline samples. Experimental data were also corrected for the sample holder and for the sample's diamagnetic contribution calculated from Pascal constants.[12] Magnetization measurements on single crystals were performed with an array of μ-SQUIDs.[13] This magnetometer works in the temperature range of 0.04 to ∼7 K and in fields of up to 1.4 T with sweeping rates as high as 10 T/s, along with a field stability of microtesla. The time resolution is approximately 1 ms. The field can be applied in any direction of the μ-SQUID plane with precision much better than 0.1° by separately driving three orthogonal coils. To ensure good thermalization, the single crystals were fixed with Apiezon grease.

Crystallography. X-ray crystallographic data were collected on a Nonius Kappa CCD diffractometer with graphite-monochromated Mo Kα radiation ($\lambda = 0.71073$ Å) at 150(2) K. A suitable crystal of **1** was picked out from the mother liquid, affixed to the end of a glass fiber using silicone grease, and quickly transferred to the goniostat where it was cooled for data collection. DENZO-SMN[14] was used for data integration, and SCALEPACK[14] corrected data for Lorentz-polarization effects. The structure was solved by direct methods and refined by a full-matrix least-squares method on F^2 using the SHELXTL crystallographic software package.[15] Due to the presence of two nonequivalent Mn_4 complexes in the structure, the possibility to transform the triclinic unit cell into a monoclinic one has been checked. On the basis of the crystal cell parameters and the systematic absence of the diffraction peaks, the triclinic symmetry and space group $P\bar{1}$ are the only possible choices considering the disordered counteranions and solvents positions in the structure.

Chart 1. Hhmp Ligand (2-Hydroxymethylpyridine)

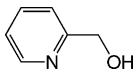

In the asymmetric unit of **1**, all four positional-disordered NO_3^- counteranions are refined with the occupancies of 70, 30, 50, and 50% for $N(31)O_3^-$, $N(31A)O_3^-$, $N(41)O_3^-$, and $N(41A)O_3^-$, respectively. Furthermore, the $N(41)O_3^-$ anion possesses an approximate 2-fold disorder with two positions, which are refined with the occupancies of 30 and 20%, respectively. There is also a disordered solvent water molecule with 50% occupancy. All of the non-hydrogen atoms were refined anisotropically except O41A atom, which is isotropically refined with fixed U_{eq} parameters. The hydrogen atoms on the parent carbon atoms were included in fixed calculated positions. The hydrogen atoms on the water molecules were located in a difference Fourier map and refined as riding on their O atom. Crystal data for **1**: $C_{36}H_{45}N_{10}O_{22.5}Mn_4$, M = 1197.58, $P\bar{1}$, $a = 10.102(2)$ Å, $b = 14.204(3)$ Å, $c = 17.338(4)$ Å, $\alpha = 83.31(3)°$, $\beta = 83.62(3)°$, $\gamma = 88.11(3)°$, $V = 2455.1(8)$ Å^3, $Z = 2$, $D_{calcd} = 1.620$ g·cm^{-3}, $\mu = 1.096$ mm^{-1}, 16 780 reflections (8605 unique, R(int) = 0.0318), 775 parameters, $R_1 = 0.0460$, $wR_2 = 0.1361$ [16 780 data, $I > 2\sigma(I)$], GOF = 1.013.

Results and Discussion

Synthesis. During recent years, many new Mn-based SMMs have been synthesized, in particular employing the Hhmp ligand (Chart 1). This ligand has been used extensively for its ability to allow the formation of polynuclear complexes such as Mn_{12},[2c] Mn_{18},[2d,16] Mn_7,[17] Mn_{10},[17b] and Mn_{21}[2l] systems with large spin ground states. Among these Mn/hmp compounds, the mixed-

(11) (a) Wernsdorfer, W.; Soler, M.; Christou, G, Hendrickson, D. N. *J. Appl. Phys.* **2002**, *91*, 7164. (b) Wernsdorfer, W.; Chakov, N. E.; Christou, G. Quantum phase interference and spin parity in Mn_{12} single-molecule magnets. http://xxx.lanl.gov/abs/cond-mat/0503193. Mar 8, 2005; *Phys. Rev. Lett.* **2005**, in press.
(12) Boudreaux, E. A.; Mulay, L. N. *Theory and Applications of Molecular Paramagnetism*; Boudreaux, E. A., Mulay, L. N., Eds.; Wiley & Sons: New York, 1976.
(13) Wernsdorfer, W. *Adv. Chem. Phys.* **2001**, *118*, 99.
(14) Otwinowski, Z.; Minor, W. *Methods Enzymol.* **1996**, *276*, 307.
(15) (a) Sheldrick, G. M. *SHELXL97*, Program for Crystal Structure Refinement; University of Göttingen: Göttingen, Germany, 1997. (b) Sheldrick, G. M. *SHELXS97*, Program for Crystal Structure Solution; University of Göttingen: Göttingen, Germany, 1997.
(16) Sañudo, E. C.; Brechin, E. K.; Boskovic, C.; Wernsdorfer, W.; Yoo, J.; Yamaguchi, A.; Concolino, T. R.; Abboud, K. A.; Rheingold, A. L.; Ishimoto, H.; Hendrickson, D. N.; Christou, G. *Polyhedron* **2003**, *22*, 2267.

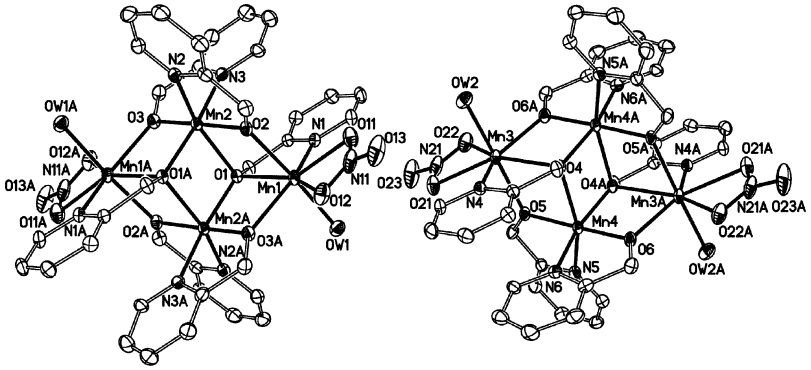

Figure 1. ORTEP representation of the cationic parts in **1** with thermal ellipsoids at 30% probability. H atoms are omitted for clarity.

valence Mn^{III}_2/Mn^{II}_2 tetranuclear complexes[18−20] possess a large $S_T = 9$ spin ground state and exhibit SMM behavior despite a few metallic centers. The same complex core has also been observed with 2,6-dihydroxymethylpyridine[2b,19,21] and triethanolamine[2m] ligands. Complex **1** has been obtained using the same synthetic procedure employed to get the first reported compound of this tetranuclear Mn/hmp-based complex series: $[Mn_4(hmp)_6Br_2(H_2O)_2]Br_2\cdot 4H_2O$.[18a,19] $Mn(NO_3)_2\cdot 4H_2O$ was used as the source of manganese ions instead of $MnBr_2\cdot 4H_2O$. In both cases, counteranions (NO_3^- or Br^-) incorporate the final structure not only as coordination-free ions to balance the charge, but also as terminal ligands on the Mn^{II} sites (vide infra). In analogous complexes of **1**, $[Mn_4(hmp)_6(NO_3)_4]\cdot CH_3CN$, and $[Mn_4(hmp)_6(CH_3CN)_2(NO_3)_2](ClO_4)_2\cdot 2CH_3CN$,[18b] the nitrate ions also act as a terminal bidentate ligand on the Mn^{II} centers but they are introduced in the second step of the reaction procedure as silver or sodium salts, respectively. Following ref 18a, the Mn nitrate salt was introduced with an excess (×2.5) of Hhmp ligand in acetonitrile with a small addition of base to help the deprotonation of the ligand and the synthesis of **1**. Complex **1** is very soluble in acetonitrile, hence a slow diffusion crystallization technique was used to obtain crystals. Diethyl ether was layered on the top of the reaction solution in sealed cylindrical (2 cm diameter) glass tubes, and red-brown needlelike crystals of **1** form after a week.

Structural Description. 1 crystallizes in the $P\bar{1}$ triclinic space group with two independent centrosymmetrical $[Mn_4(hmp)_6(H_2O)_2(NO_3)_2]^{2+}$ cations (Figure 1). In addition to these tetranuclear complexes, the unit cell contains also four disordered nitrate ions and five water molecules. In the cationic complexes, Mn ions are arranged in a double-cuboidal fashion where Mn(1) and Mn(3) are heptacoordinated and Mn(2) and Mn(4) are hexacoordinated.

This core geometry and coordination modes have been already observed in related materials.[2b,m,18−21] The oxidation states of the Mn ion sites can be easily assigned as trivalent for Mn(2) and Mn(4), and divalent for Mn(1) and Mn(3), based on charge balance consideration and bond valence sum calculation.[22] One hmp ligand is coordinated to each Mn^{II} site by the N (N(1) and N(4)) of the aromatic ring and hold together this Mn^{II} with its two neighbor Mn^{III} ions by its oxygen atom (O(1) and O(4)) in a μ_3-bridging mode. On the other hand, the coordination sphere of each Mn^{III} metal ions is occupied by two monoanionic bidentate hmp ligands which link them to their neighbor Mn^{II} ions by a μ-oxygen bridge. Moreover, the coordination sphere of the Mn^{II} ions is completed by one water molecule and an NO_3^- anion acting as a bidentate ligand as already observed in $[Mn_4(hmp)_6(NO_3)_4]\cdot CH_3CN$ or $[Mn_4(hmp)_6(CH_3CN)_2(NO_3)_2](ClO_4)_2\cdot 2CH_3CN$.[18b] As expected, Mn^{III} ions possess Jahn−Teller (JT) elongation axes, [N(2)−Mn(2)−O(1)] and [N(5)−Mn(4)−O(4)], which are slightly bent with angles of 158.48(1)° and 157.65(1)°, respectively. The two cationic parts and their average JT axes[23] display different orientations separated by an angle close to 12.1°. In the crystal packing, counteranions, interstitial solvent molecules, and the Mn_4 shell are closely packed through various weak H-bonding interactions that stabilize the structure. Nevertheless, it is important to note that direct hydrogen bonding or $\pi-\pi$ stacking between Mn_4 units is absent in the packing. This feature is clearly in contrast with the direct Br···Br contact or $\pi-\pi$ interactions between Mn_4 units observed in $[Mn_4(hmp)_6Br_2(H_2O)_2]Br_2\cdot 4H_2O$[18a] and $[Mn_4(hmp)_6(CH_3CN)_2(NO_3)_2](ClO_4)_2\cdot 2CH_3CN$,[18b] respectively.

High-Temperature Magnetic Properties. dc magnetic susceptibility measured on a polycrystalline sample of **1** is depicted in Figure 2. The χT product increases from 14.7 $cm^3\cdot K\cdot mol^{-1}$ at ambient temperature to reach a maximum of 35.5 $cm^3\cdot K\cdot mol^{-1}$ at 4.7 K and then decreases slightly to 32.2 $cm^3\cdot K\cdot mol^{-1}$ at 1.82 K. This behavior is typically observed for $[Mn_4(hmp)_6]^{4+}$ complexes exhibiting ferromagnetic intracluster interactions noted J_{bb} between Mn^{3+} ions and J_{wb} between Mn^{2+} and Mn^{3+} ions. Then, the fall of χT at lower temperature is a consequence of zero-field splitting (ZFS) of the lowest spin states or weak antiferromagnetic intermolecular interactions (vide infra). At high temperature, the χT versus T data were simulated using the Heisenberg−Van Vleck model and the following spin Hamiltonian: $H = -2J_{bb}(S_{Mn^{3+}}S_{Mn^{3+}(A)}) - 2J_{wb}(S_{Mn^{3+}} + S_{Mn^{3+}(A)})(S_{Mn^{2+}} + S_{Mn^{2+}(A)})$, already employed by Christou and

(17) (a) Bolcar, M. A.; Aubin, S. M. J.; Folting, K.; Hendrickson, D. N.; Christou, G. *Chem. Commun.* **1997**, *15*, 1445. (b) Harden, N. C.; Bolcar, M. A.; Wernsdorfer, W.; Abboud, K. A.; Streib, W. E.; Christou, G. *Inorg. Chem.* **2003**, *42*, 7067.
(18) (a) Yoo, J.; Yamaguchi, A.; Nakano, M.; Krystek, J.; Streib, W. E.; Brunel, L. C.; Hishimoto, H.; Christou, G.; Hendrickson, D. N. *Inorg. Chem.* **2001**, *40*, 4604. (b) Yang, E. C.; Harden, N.; Werndorfer, W.; Zakhrov, L.; Brechin, E. K.; Rheingold, A. L.; Christou G.; Hendrickson, D. N. *Polyhedron* **2003**, *22*, 1857.
(19) Hendrickson, D. N.; Christou, G.; Ishimoto, H.; Yoo, J.; Brechin, E. K.; Yamaguchi, A.; Rumberger, E. M.; Aubin, S. M. J.; Sun Z.; Aromí, G. *Polyhedron* **2001**, *20*, 1479.
(20) Lecren, L.; Li, Y.-G.; Wernsdorfer, W.; Roubeau, O.; Miyasaka, H.; Clérac, R. *Inorg. Chem. Commun.* **2005**, *8*, 628.
(21) Brechin, E. K.; Yoo, J.; Nakano, M.; Huffman, J. C.; Hendrickson, D. N.; Christou, G. *Chem. Commun.* **1999**, *17*, 783.
(22) Brown, I. D.; Altermatt, D. *Acta Crystallogr., Sect. B* **1985**, *41*, 244.
(23) On a Mn_4 unit, Mn^{III} JT axes are parallel, defining the preferential orientation of the Mn^{III} magnetic spin, also called the local easy direction.

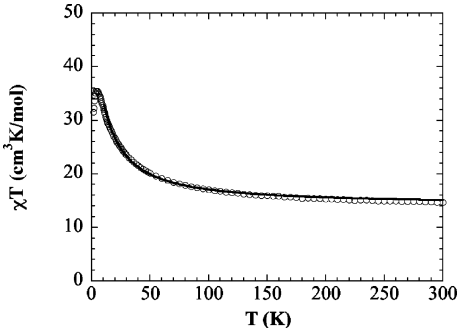

Figure 2. Plot of χT vs T under 0.1 T (○). The solid line represents the best fit obtained with the tetranuclear model described in the text. Data below 15 K were omitted in the fitting procedure to avoid the influence of antiferromagnetic intertetramer interactions or magneto-anisotropic effects.

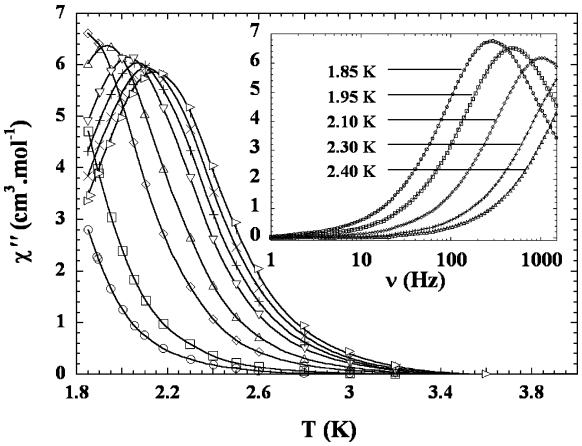

Figure 3. Plot of χ'' vs T under zero dc field (○ 50 Hz, □ 99.947 Hz, ◇ 299.52 Hz, △ 498.67 Hz, ▽ 801.28 Hz, + 997.34 Hz, × 1201.9 Hz, | 1399.3 Hz, side △ 1488.1 Hz). Inset: Plot of χ'' vs ν under zero dc field. Solid lines are guides.

Hendrickson et al.[18a] Above 15 K, a good fit was achieved with $g = 1.96$, $J_{wb}/k_B = +0.80(5)$ K, and $J_{bb}/k_B = +7.1(1)$ K (solid line in Figure 2), consistent with the values reported in the literature.[2b,m,18,20] Hence, this set of ferromagnetic couplings between Mn ions induces for **1** an $S_T = 9$ ground state with an $S_T = 8$ first excited state lying 6.4 K above.

Relaxation Time of the Magnetization: Thermal versus Quantum Relaxation Processes. As expected based on the magnetic properties of analogous compounds,[18,19] **1** should display SMM behavior. Thus, the slow relaxation of the magnetization was probed using ac and dc measurements (Figures 3 and 4). As expected for SMMs, the ac susceptibility is strongly frequency-dependent, and remarkably for a Mn_4/hmp SMM, blocking temperatures are observed above 1.80 K for $\nu_{ac} > 300$ Hz.[18−20] In this temperature domain, the relaxation time (τ) is thermally activated with $\Delta_{eff}/k_B = 20.9$ K and $\tau_0 = 6.7 \times 10^{-9}$ s (inset Figure 3). Note that Δ_{eff} is surprisingly high for a compound of this family (which is usually found around 15−18 K),[18,19] but still lower than the expected barrier: $\Delta/k_B = |D|S_T^2/k_B = 28.4$ K (with $D/k_B = -0.35$ K determined from M versus H measurements, vide infra). Experimentally, in this temperature domain, the two relaxation processes (thermal and quantum) are in competition. Hence, the thermal barrier is "short-cut" by the quantum tunneling of the magnetization, and an effective energy barrier (Δ_{eff}) on the relaxation time is measured smaller than the theoretical one. In the case of **1**, the "short-cut" of the barrier by tunneling is thus less efficient than

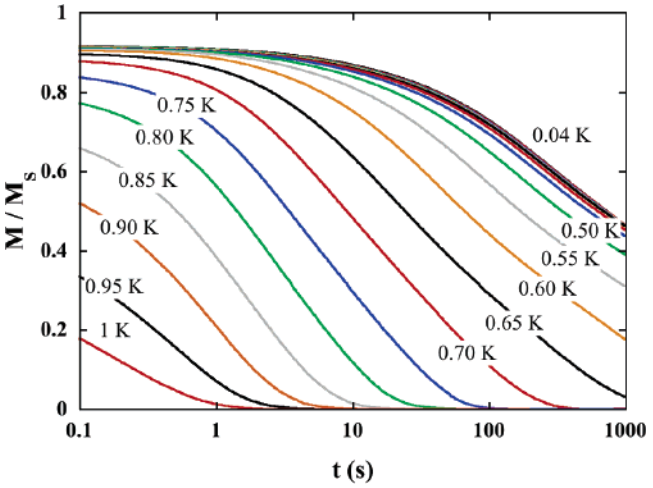

Figure 4. Relaxation of the magnetization at different temperatures. The data are normalized to the saturation magnetization (M_s) at 1.4 T.

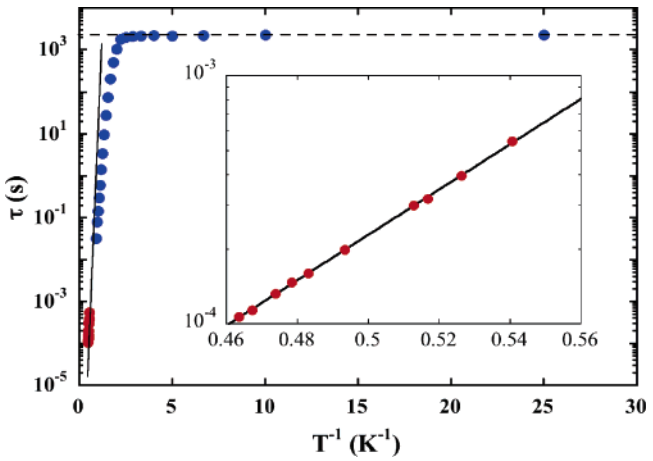

Figure 5. τ vs T^{-1} plot determined by dc (blue ●) and ac (red ●) techniques. Inset: τ vs T^{-1} plot using ac data. The solid line represents the Arrhénius fit.

that in other Mn_4/hmp complexes.[18,19] With lowering temperature, the relaxation time becomes too slow to be studied with ac measurements in the available range of frequencies. Therefore, direct measurements of the magnetization relaxation were performed down to 0.04 K (Figure 4). All the $M/M_s(t)$ curves can be scaled into a single master curve. The relaxation time τ was extracted at each temperature taking $\tau = t$ when $M/M_s(t)$ reaches $1/e$ (blue dots in Figure 5). Therefore, below 1 K, the relaxation time does not follow anymore an Arrhénius law and saturates as expected when quantum tunneling of the magnetization (QTM) is the dominant (fastest) pathway of relaxation (Figure 5). Thus, QTM regime is observed below 0.34 K with a characteristic time of $\tau_{QTM} = 2300$ s (Figure 5, dotted line). This value contrasts with the 1000 s measured for $[Mn_4(hmp)_6Br_2(H_2O)_2]Br_2 \cdot 4H_2O$,[19] suggesting that the transverse anisotropy (E), which governs τ_{QTM}, is reduced in **1**, although the Mn_4O_6 cores possess the same local symmetry.

Uniaxial Anisotropy *D* and Intercomplex Interactions. The uniaxial anisotropy D of **1** and intermolecular antiferromagnetic interactions have been determined from M versus H data measured below 1.5 K on a single crystal using the μ-SQUID technique.[13] The position of the magnetic axes on the oriented single crystals has been determined rotating the magnetic field in different planes and measuring the M versus H response. This

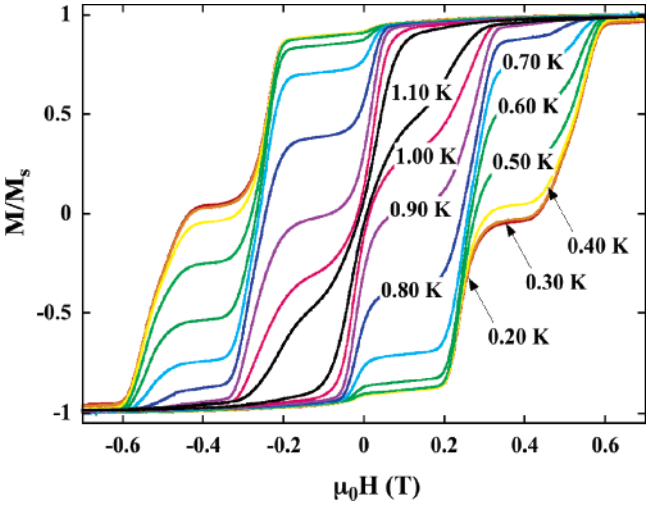

Figure 6. Magnetization hysteresis loops in the 1.10−0.04 K range at a 0.07 T/s sweep rate in the average easy direction of a mono-crystal of **1**.

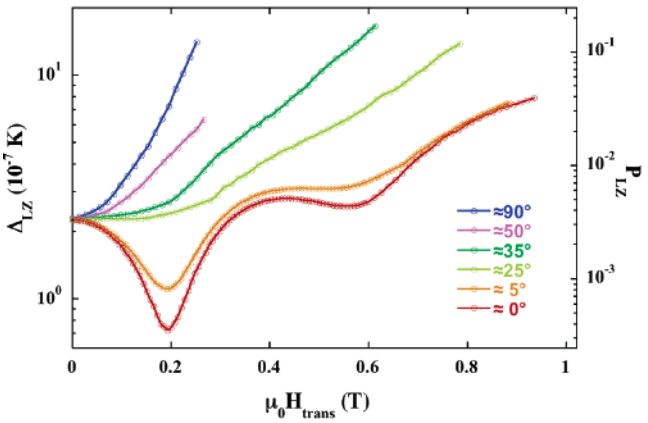

Figure 7. Tunnel splitting (Δ_{LZ}) and tunnel probability (P_{LZ}) as a function of the transverse field rotated in the *xy* plane of the crystal (average hard direction: 0°; average intermediate direction: 90°) for the $m_S = \pm 9$ quantum transition at 40 mK and a field sweep rate of 0.28 T/s. Solid lines are guides.

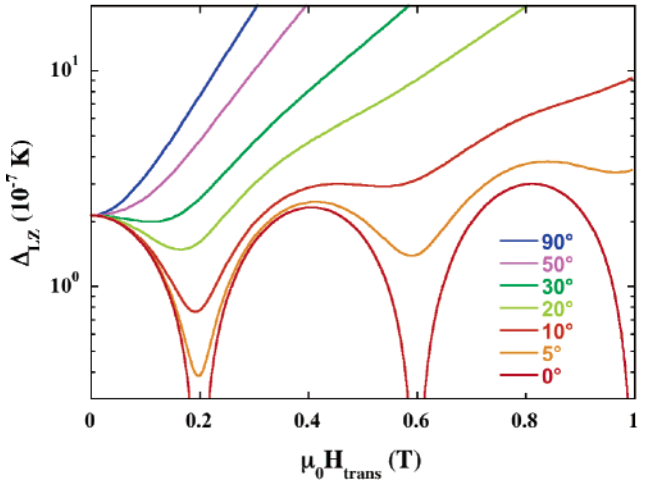

Figure 8. Calculated tunnel splitting Δ_{LZ} as a function of transverse field for the quantum transition between $m_S = \pm 9$ at several azimuth angles (in the *xy* plane).

study revealed the presence of two sets of magnetic axes as expected for the presence of two independent Mn_4 complex orientations with different local tensors of anisotropy. As shown in Figure 6, slow relaxation of the magnetization and hence hysteresis loops are observed below 1.20 K when the field is applied along the average easy axis direction. The coercive field varies strongly with temperature until 0.30 K where it becomes temperature-independent but staying field sweep rate-dependent, even at 0.04 K, as expected for ground-state tunneling.

The regular steps of the loops correspond to resonant tunneling transitions between $m_S = 9$ and $m_S = -9$ (at −0.02 T), $m_S = -8$ (at 0.24 T), and $m_S = -7$ (at 0.50 T). The small shift of the $m_S = \pm 9$ transition from zero field confirms the presence of very weak inter-SMM interactions ($zJ'/k_B \approx -1.5 \times 10^{-3}$ K).[18b] It is worth noting that these interactions are small compared to those for $[Mn_4(hmp)_6Br_2(H_2O)_2]Br_2 \cdot 4H_2O$, which shows a three-dimensional antiferromagnetic order below 1.33 K,[24] or for $[Mn_4(hmp)_6(CH_3CN)_2(NO_3)_2](ClO_4)_2 \cdot 2CH_3CN$, which possesses exchange interactions of the order of 10^{-2} K.[18b] From the field separation between steps ($\Delta H \approx 0.26$ T) and eq 3, D/k_B is estimated at −0.35 K, in good agreement with the values reported for similar complexes using reduced magnetization technique or high-field EPR.[18] Moreover, because the angle between the two local easy axes is small (12.1°), it is important to note that its influence of the order of ±0.5% (cos(6°) = 0.995) onto the determination of *D* can be neglected.

Quantum Phase Interference: Transverse Anisotropy *E*. To get an estimation of *E*, we used the Landau−Zener method.[9a,11] Indeed, as illustrated in the Introduction by Scheme 1, when the spin Hamiltonian contains transverse terms such as $E(S_{Tx}^2 - S_{Ty}^2)$, crossings of the spin levels are avoided with an energy gap called tunnel splitting, Δ_{LZ}. Experimentally, the tunnel probability (P_{LZ}) can be estimated, and hence, the tunnel splitting can be calculated using the Landau−Zener equation[9a] (see eq 4). The fraction of Mn_4 complexes that reverse their spin is directly measured by saturating the magnetization of the crystal under a large negative field (typically −1.4 T) at 0.04 K and sweeping the longitudinal applied field at a constant rate of 0.28 T/s over the zero field resonance transition ($m_S = \pm 9$). This procedure was then repeated in the presence of the transverse applied field at different values (between 0 and 0.9 T) and directions in the *xy* plane (Figure 7). In the case of very small tunnel probability, the field was swept back and forth over the zero-field resonance until a larger fraction of molecules reversed their spin. A scaling procedure yields the probability for only one sweep.[9a] When applying H_{trans} along the average hard direction, oscillations of the tunnel splitting due to constructive or destructive quantum spin phase interference of two tunnel pathways (Scheme 1c) are observed (Figure 7).[10] As expected for integer spin ground state and as already seen for $[Fe_8O_2(OH)_{12}(tacn)_6]^{8+}$, the tunnel splitting displays a maximum when the transverse field is zero. This value obtained for **1** is around 3×10^{-7} K, about three times larger than that in the Fe_8 SMM.[9a] As shown in Figure 7, the tunnel splitting also oscillates when the transverse field is applied along the average hard axis. As expected with this anisotropy symmetry (eq 2), these oscillations progressively vanish when rotating the transverse field from *x* to *y* directions. Looking at the data obtained in the average hard direction, we could estimate the oscillation period, ΔH_{LZ}, to be 0.40 T, leading to $E/k_B = +0.083$ K (using eq 5 with $D/k_B = -0.35$ K and $g = 1.96$). A numerical

(24) Yamaguchi, A.; Kusumi, N.; Ishimoto, H.; Mitamura, H.; Goto, T.; Mori, N.; Nakano, M.; Awaga, K.; Yoo, J.; Hendrickson, D. N.; Christou, G. *J. Phys. Soc. Jpn.* **2002**, *71*, 414.

diagonalization of the Hamiltonian of the $S_T = 9$ spin system, described by a [19 × 19] matrix, allows a qualitative simulation of the experimental data (Figure 8). The value of Δ_{LZ} at $H_{trans} = 0$ and the periodicity of oscillation are quantitatively reproduced for $|D/k_B| = 0.35$ K and $E/k_B = +0.083$ K, in perfect agreement with the above values. Moreover, it should be noted that the Δ_{LZ} oscillations are less pronounced than the theoretical ones. This effect is mainly due to the presence of the two Mn_4 units in the unit cell that have hard axes being not completely parallel (with an angle estimated at about 10° from μ-SQUID measurements) and to the weak inter-Mn_4 interactions. However, because the angle between hard directions is small, its influence of a maximum of 1.5% (i.e., cos(10°) = 0.985) onto the determination of E can be easily neglected.

Concluding Remarks

After more than 15 years since the discovery of the first SMM,[1] more than 100 SMMs have been reported. Nevertheless, the complexes of the so-called Mn_{12} family, $[Mn_{12}O_{12}(O_2CR)_{16}(H_2O)_4]$, are still the most attractive examples in this field. Two main reasons explain the popularity of these compounds: (i) it is easy to synthesize very stable derivatives and (ii) Mn_{12} systems are still continuing to reveal unique physical properties (slow relaxation of the magnetization, resonant quantum tunneling, quantum phase interference, etc.). These two reasons have pushed scientists to develop jointly the chemistry and the physics of this amazing system. From this point of view and as illustrated by the present work, the Mn_4/hmp SMM complexes form a new family of complexes that fulfills the above appealing assets of the Mn_{12} series. Christou and Hendrickson have synthesized the first complex of this family, $[Mn_4(hmp)_6Br_2(H_2O)_2]Br_2\cdot 4H_2O$, and more recently few derivatives exhibiting SMM behavior.[18,19] In this work, we have been able to extend their findings by obtaining a new Mn_4/hmp derivative, $[Mn_4(hmp)_6(H_2O)_2(NO_3)_2](NO_3)_2\cdot 2.5H_2O$ (**1**), and studying in detail its SMM behavior down to 0.04 K, while the original complex, $[Mn_4(hmp)_6Br_2(H_2O)_2]Br_2\cdot 4H_2O$, displays a three-dimensional antiferromagnetic order below 1.33 K.[24] The two relaxation modes of its magnetization, thermal and quantum, have been described. In addition, for the first time in this family of compounds, quantum phase interference has been observed. This rarely observed quantum phenomenon and the complete set of measurements reported here have allowed us to estimate the intra- ($J_{wb}/k_B = +0.80(5)$ K and $J_{bb}/k_B = +7.1(1)$ K) and inter- ($zJ'/k_B \approx -1.5 \times 10^{-3}$ K) complex interactions, the anisotropic parameters ($D/k_B = -0.35$ K and $E/k_B = +0.083$ K), and the tunnel splitting ($\Delta_{LZ} = 3 \times 10^{-7}$ K when $H_{trans} = 0$ Oe) of **1**. It is particularly interesting to note that E is significantly reduced in **1** compared to that in $[Mn_4(hmp)_6Br_2(H_2O)_2]Br_2\cdot 4H_2O$, with $E/k_B = 0.124$ K determined by high-field EPR.[18a] Indeed, this decrease of the transverse anisotropy results in a slowing down of the QTM characteristic relaxation time (τ_{QTM}) and an enhancement of the effective energy barrier (Δ_{eff}) observed in **1**. To conclude, it should be mentioned that this new Mn_4/hmp derivative is the smallest complex to show all the known characteristic features for an SMM (thermal relaxation, ground-state quantum tunneling, and resonant quantum tunneling of the magnetization, quantum phase interference), opening new perspectives to understand, for example, the influence of the excited states on these quantum phenomena.

Acknowledgment. This work was supported by PRESTO and CREST projects, Japan Science and Technology Agency, Grant-in-Aid from the Ministry of Education, Culture, Sports, Science, and Technology (Japan), the EC-TMR Network "QuEMolNa" (MRTN-CT-2003-504880), the CNRS, the University of Bordeaux 1, and the Conseil Régional d'Aquitaine.

Supporting Information Available: Crystal data and structure refinement for **1**, atomic coordinates and equivalent isotropic displacement parameters for **1**, bond lengths and angles for **1**, anisotropic displacement parameters for **1**, and hydrogen coordinates and isotropic displacement parameters for **1** (PDF). X-ray crystallographic file of **1** (CIF). This material is available free of charge via the Internet at http://pubs.acs.org. The CIF file is also available on application to the Cambridge Data Centre, 12 Union Road, Cambridge CB21EZ, U.K. (fax: (+44) 1223-336-033; email: deposit@ccdc.cam.ac.uk), CCDC 263143.

JA050994Z